International Journal of Engineering Research and Development
e- ISSN: 2278-067X, p-ISSN: 2278-800X, www.ijerd.com
Volume 22, Issue 7 (July 2026), PP 12-19

Vibroacoustic Response of a Finite Double-Composite Plate Filled with an Air Cavity in Thermal Environment

Phung Xuan Son[1]*, Pham Ngoc Thanh[1] and Vu Thi Hue[1]
[1]*Hanoi University of Industry, Tay Tuu district, Ha Noi, Viet Nam*
**Corresponding Author*

ABSTRACT
This work develops an analytical framework based on classical laminated plate theory to characterize the vibroacoustic behavior of finite, simply supported, orthotropic double-panel composite structures enclosing an air cavity. The coupled system is subjected to simultaneous thermal fields and harmonic wave excitations. By leveraging the modal decomposition technique, the governing equations are solved using a double Fourier series approach to map the acoustic insulation metrics of the panel. The sound transmission loss (STL) is quantified via the ratio of incident to transmitted acoustic powers. After demonstrating the model's accuracy through a comparative validation with previously published literature, a comprehensive parametric sweep is executed. This systematic evaluation details how critical design variables—specifically composite tailoring, air cavity thickness, and the lamination scheme—govern the sound transmission loss characteristics.
Keywords: *Simply supported, Sound transmission loss, Thermal loads*

Date of Submission: 22-06-2026 Date of acceptance: 03-07-2026

I. INTRODUCTION

The double-plate is widely used in construction structures, ships, turbofan, aerospace, etc. Therefore, research on the sound insulation capacity of double-plate has received much attention from researchers worldwide. For decades, the vibroacoustic behavior of an infinite or finite double-plates is an interesting research topic with different approaches used. Kropp and Rebillard [1] focused their research on optimizing the sound insulation performance of infinite isotropic metallic double-plates within the low-frequency range. Their study categorized the low-frequency band into three distinct regimes based on whether the panel's resonance frequency was significantly lower than, higher than, or close to the critical frequency of the structure. Villot et al. [2] investigated the computation of reflected and transmitted sound fields for infinite isotropic metallic double-panels excited by airborne plane waves. This methodology yielded theoretical predictions that aligned far more closely with experimental measurements than conventional classical wave approaches applied to infinite single-plate structures.

Shifting the focus to bounded configurations, Craik [3] examined sound transmission across finite isotropic metallic double-plates utilizing the Statistical Energy Analysis (SEA) method. The presented theoretical framework leveraged an infinite plate model to determine the forced response of the panel, combined with the radiation efficiency of a finite plate. Furthermore, Carneal and Fuller [4, 5] conducted both theoretical and experimental investigations into the vibroacoustic behavior of finite, rectangular, isotropic aluminum double-panels under simply supported boundary conditions on all four edges.

Concurrently, their experimental model incorporated an Active Structural Acoustic Control (ASAC) approach implemented on clamped aluminum double-plates. Lastly, Chazot and Guyader [6] studied the sound transmission loss of finite isotropic aluminum double-panels enclosing an air cavity under simply supported constraints by employing a patch-mobility method. In their work, the plate structure was driven by patch pressures that accounted for both the room geometry and the specific location of the acoustic source. Lu and Xin [7] presented an analytical approach to investigate the sound transmission across rectangular metallic (isotropic) double-panel structure containing an air cavity under various boundary constraints by using the method of modal function and the weighted residual (Galerkin) method. Liu and Li [8, 9] obtained the vibration and acoustic response of a rectangular isotropic sandwich plate which is subjected to a concentrated harmonic force under thermal environment by using the analytical formulations based on equivalent non-classical theory.

However, few researchers studied the STL of the sandwich panels in thermal environment. And most of theories are cumbersome even impossible to obtain the analytical solutions of STL for laminated composite plates in thermal environment as they need too many unknowns. Recently, the authors presented a piecewise shear deformation theory [10] for sandwich panels and investigated the vibration and acoustic responses of the sandwich panels exerted on a concentrated harmonic force in a high temperature environment [11]. Thanh and

Thinh [12, 13] studied the vibroacoustic behavior of an orthotropic laminated composite rectangular plate with simply supported and clamped boundary conditions under a sound wave excitation in thermal environments by applying the classic thin-plate theory. An improved analytical procedure has been developed that allows for an efficient solution of the finite composite plate sound transmission problem.

The objective of this study is to develop a model to describe accurately the sound transmission loss across a finite simply supported laminated double-composite plate filled with air cavity in thermal environment. Thereby, assessing the influence of several key system parameters on sound transmission loss including the composite materials, the air cavity thickness and the lamination scheme are systematically examined.

II. THEORETICAL FORMULATION

2.1. Plate geometry and assumptions

The finite-sized, double-plate partition with air cavity is assumed to be rectangular, baffled, and simply supported along its boundaries, occupying the spatial region ($0 < x < a$, $0 < y < b$, $0 < z < H$) in Cartesian coordinates. The bottom and upper plates (Fig. 1) have thicknesses h and are separated by an air cavity of thickness H. The double-plate partition divides the space into two regions, i.e. the incident sound wave region ($z < 0$) and the transmitted sound wave region ($z > H + 2h$).

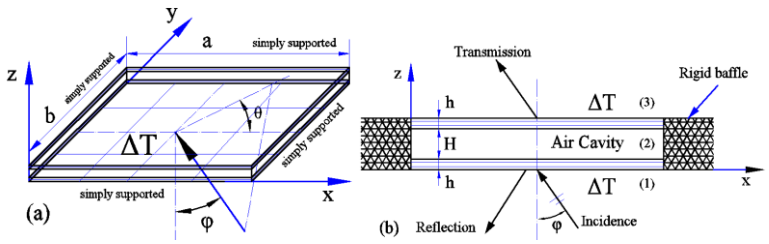

Figure 1: Schematic of sound transmission loss through a baffled and simply supported double-plate partition: (a) Global view and (b) side view along the arrow direction in (a).

Let a uniform plane sound wave varying harmonically in time impinge on the bottom plate with incident angle φ and azimuth angle θ. Vibration of the bottom plate due to harmonic sound excitation alters dynamically the pressure field within the hermetical air cavity. The incidence field contains three components, i.e., the incidence pressure, the reflection pressure, and the transmission pressure.

2.2. Governing equations

The vibroacoustic response of a double-plate partition with air cavity (Fig. 1) is induced by sound pressure fluctuations and differences between two adjacent fields (above and below each plate) and is governed by [12, 13]:

$$D_{11}\frac{\partial^4 w_1(x,y;t)}{\partial x^4}+2\left(D_{12}+2D_{66}\right)\frac{\partial^4 w_1(x,y;t)}{\partial x^2\partial y^2}+D_{22}\frac{\partial^4 w_1(x,y;t)}{\partial y^4}+m^*\frac{\partial^2 w_1(x,y;t)}{\partial^2 t}$$
$$-\left(N_1\frac{\partial^2 \mathrm{w}(x,y;t)}{\partial x^2}+N_2\frac{\partial^2 \mathrm{w}(x,y;t)}{\partial y^2}\right)=j\omega\rho_0\left[\Phi_1(x,y,z;t)-\Phi_2(x,y,z;t)\right] \quad (1)$$

$$D_{11}\frac{\partial^4 w_1(x,y;t)}{\partial x^4}+2\left(D_{12}+2D_{66}\right)\frac{\partial^4 w_1(x,y;t)}{\partial x^2\partial y^2}+D_{22}\frac{\partial^4 w_1(x,y;t)}{\partial y^4}+m^*\frac{\partial^2 w_1(x,y;t)}{\partial^2 t}$$
$$-\left(N_1\frac{\partial^2 \mathrm{w}(x,y;t)}{\partial x^2}+N_2\frac{\partial^2 \mathrm{w}(x,y;t)}{\partial y^2}\right)=j\omega\rho_0\left[\Phi_2(x,y,z;t)-\Phi_3(x,y,z;t)\right] \quad (2)$$

Where: D_{ij} *(ij = 11, 12, 66, 22)* is the flexural rigidity, m^* is the surface density of the plate, ρ_0 is the air density, ω is the angular frequency of the incident sound and $\Phi_i(i=1,2)$ are the velocity potentials for the incident field and the transmitted field, respectively.N_i *(i = 1, 2)* are constants determined [12, 13]

$$N_i=\sum_{k=1}^{N}\int_{z_{k-1}}^{z_k}[Q_{ij}]_k\alpha_j\Delta T dz \qquad (i,j=1,2) \quad (3)$$

Where: α_j *(j = 1, 2)* are coefficients of thermal expansion in longitudinal and transverse direction; ΔT is temperature difference (assumed to be constant in this study). The flexural rigidity of laminated composite plate is determined by Eq. (4),

$$D_{ij} = \frac{1}{3}\sum_{k=1}^{n} Q_{ij}^{k}\left(z_{k+1}^{3} - Z_{k}^{3}\right) \tag{4}$$

Where: Q_{ij} *(ij = 11, 12, 66, 22)* are the reduced stiffnesses of the k[th] layer; E_1, E_2, G_{12}, ν_{12} are the elastic constants of the k[th] layer.

The displacement of the double-plate composite plate induced by the incident sound is expressed as Eqs. (5) and (6).

$$w_1(x,y;t) = w_{01}.e^{-j(k_x x + k_y y - \omega t)} \tag{5}$$

$$w_2(x,y;t) = w_{02}.e^{-j(k_x x + k_y y - \omega t)} \tag{6}$$

The acoustic velocity potential in the incidence field (Fig. 1) is defined as Eq. (7),

$$\Phi_1(x,y,z;t) = I.e^{-j(k_x x + k_y y + k_z z - \omega t)} + \beta.e^{-j(k_x x + k_y y - k_z z - \omega t)} \tag{7}$$

Where I and β are the amplitudes of the incident (positive-going) and the reflected (negative-going) waves, respectively. Similarly, the velocity potential in the air cavity is given by Eq. (8),

$$\Phi_2(x,y,z;t) = \varepsilon.e^{-j(k_x x + k_y y + k_z z - \omega t)} + \psi.e^{-j(k_x x + k_y y - k_z z - \omega t)} \tag{8}$$

Where ε is the amplitude of the positive-going wave and ψ is the amplitude of the negative-going wave. The velocity potential in the transmitting (radiating) waves is given by Eq. (9),

$$\Phi_3(x,y,z;t) = \gamma.e^{-j(k_x x + k_y y + k_z z - \omega t)} \tag{9}$$

Where ξ is the amplitude of the transmitting (positive-going) wave.

These wave numbers are determined by the elevation angle φ and azimuth angle θ of the incident sound wave as given by Eq. (10),

$$k_x = k_0 \sin\varphi\cos\theta; k_y = k_0 \sin\varphi\sin\theta; k_z = k_0\cos\varphi \tag{10}$$

Where $k_0 = \omega/c_0$ is the acoustic wave number in air and c_0 is the acoustic speed in the air.

With the plate fully simply supported onto a rigid baffle, the boundary conditions can be expressed as Eq. (11).

$$x = 0,\ a,\quad w_1 = w_2 = 0,\quad \frac{\partial^2 w_1}{\partial x^2} = \frac{\partial^2 w_2}{\partial x^2} = 0\ ;\qquad \mathrm{y} = 0,\ \mathrm{b},\quad \mathrm{w}_1 = w_2 = 0,\ \frac{\partial^2 w_1}{\partial y^2} = \frac{\partial^2 w_2}{\partial y^2} = 0 \tag{11}$$

At the air-plate interface the normal velocity is continuous, yielding the corresponding velocity compatibility condition equations given by Eq. (12).

$$z = 0,\quad -\frac{\partial \Phi_1}{\partial z} = j\omega w_1;\ -\frac{\partial \Phi_2}{\partial z} = j\omega w_1;\qquad z = h,\quad -\frac{\partial \Phi_2}{\partial z} = j\omega w_2;\ -\frac{\partial \Phi_3}{\partial z} = j\omega w_2 \tag{12}$$

The flexural motions of the bottom and upper plates induced by a time-harmonic incident plate sound wave can be expressed in the form of double series as Eq. (13),

$$w_1(x,y;t) = \sum_{m=1}^{\infty}\sum_{n=1}^{\infty}\phi_{mn}(x,y)q_{1,mn}(t); w_2(x,y;t) = \sum_{m=1}^{\infty}\sum_{n=1}^{\infty}\phi_{mn}(x,y)q_{2,mn}(t) \tag{13}$$

Where the modal function φ^{mn} and modal coefficients $q_{i,}^{mn}$ (i = 1, 2) are given by Eq. (14),

$$\phi_{mn}(x,y) = \sin\frac{2m\pi x}{a}\sin\frac{2n\pi x}{b};\ q_{1,mn}(t) = \alpha_{1,mn}e^{j\omega t},\quad q_{2,mn}(t) = \alpha_{2,mn}e^{j\omega t} \tag{14}$$

Where $\alpha_{1,mn}$ and $\alpha_{2,mn}$ are the modal coefficients of the bottom plate and the upper plate, respectively.

Accordingly, the velocity potentials for the sound incident region, air cavity, and sound transmitting region may be expressed as Eqs. (15) and (16),

$$\Phi_1(x,y,z;t)=\sum_{m=1}^{\infty}\sum_{n=1}^{\infty}I_{mn}\varphi_{mn}e^{-j(k_z z-\omega t)}+\sum_{m=1}^{\infty}\sum_{n=1}^{\infty}\beta_{mn}\varphi_{mn}e^{-j(-k_z z-\omega t)} \tag{15}$$

$$\Phi_2(x,y,z;t)=\sum_{m=1}^{\infty}\sum_{n=1}^{\infty}\varepsilon_{mn}\phi_{mn}e^{-j(k_z z-\omega t)}+\sum_{m=1}^{\infty}\sum_{n=1}^{\infty}\psi_{mn}\phi_{mn}e^{-j(-k_z z-\omega t)};\ \Phi_3(x,y,z;t)=\sum_{m=1}^{\infty}\sum_{n=1}^{\infty}\gamma_{mn}\phi_{mn}e^{-j(k_z z-\omega t)} \tag{16}$$

Where the coefficients I^{mn}, β^{mn}, ε^{mn}, ψ^{mn} and γ^{mn} are determined by the Fourier cosine transform as Eq. (17). From Eqs. (13) and (17),

$$\chi_{mn}=\frac{4}{ab}\int_0^b\int_0^a \chi e^{-j(k_x x+k_y y)}\sin\frac{2m\pi x}{a}\sin\frac{2n\pi x}{b}dxdy \tag{17}$$

the relation between coefficients I^{mn} and I_0 is obtained as Eq. (18).

$$I_{mn}=\frac{4I_0 mn\pi^2\left\{1-(-1)^m e^{-jk_x a}-(-1)^n e^{-jk_y b}+(-1)^{m+n}e^{-j\left(k_x a+k_y b\right)}\right\}}{\left(k_x^2a^2-m^2\pi^2\right)\left(k_y^2b^2-n^2\pi^2\right)} \tag{18}$$

Using the displacement continuity condition at air-plate interfaces and Bernoulli's equation [7, 12, 13], substituting Eqs. (15)–(16) into Eqs. (13) leads to Eqs. (19) and (20).

$$\beta_{mn}=I_{mn}-\frac{\omega}{k_z}\alpha_{1,mn};\ \varepsilon_{mn}=\frac{\omega\left(\alpha_{1,mn}e^{jk_z H}-\alpha_{2,mn}\right)}{k_z\left(e^{-jk_z(h-H)}-e^{-jk_z(H+h)}\right)} \tag{19}$$

$$\psi_{mn}=\frac{\omega\left(\alpha_{2,mn}-\alpha_{1,mn}e^{-jk_z H}\right)}{k_z\left(e^{jk_z(h-H)}-e^{jk_z(H+h)}\right)};\ \gamma_{mn}=\frac{\omega\alpha_{2,mn}e^{jk_z(H+2h)}}{k_z} \tag{20}$$

Substituting Eqs. (14) and (19)–(20) into Eqs. (1) and (2) and applying the orthogonal properties of modal functions, one gets Eqs. (21) and (22),

$$\ddot{q}_{1,mn}(t)+\omega_{1,mn}^2 q_{1,mn}(t)-\frac{j\omega\rho_0}{m^*}\left[\begin{array}{l}\left(I_{mn}-\varepsilon_{mn}\right)e^{-j(k_z z-\omega t)}+\left(\beta_{mn}-\psi_{mn}\right)e^{-j(-k_z z-\omega t)}\\ +\,4N_1\left(\frac{m\pi}{a}\right)^2+4N_2\left(\frac{n\pi}{b}\right)^2\end{array}\right]=0 \tag{21}$$

$$\ddot{q}_{2,mn}(t)+\omega_{2,mn}^2 q_{2,mn}(t)-\frac{j\omega\rho_0}{m^*}\left[\begin{array}{l}\left(\varepsilon_{mn}-\gamma_{mn}\right)e^{-j(k_z z-\omega t)}+\psi_{mn}e^{-j(-k_z z-\omega t)}\\ +\,4N_1\left(\frac{m\pi}{a}\right)^2+4N_2\left(\frac{n\pi}{b}\right)^2\end{array}\right]=0 \tag{22}$$

where $\omega_{i,mn}$ (i = 1, 2) are the natural frequencies of the two single-leaf plates determined by Eq. (23).

$$\omega_{i,mn}^2=\frac{\pi^4}{m^*b^4}\left[D_{11}m^4\left(\frac{b}{a}\right)^4+2\left(D_{12}+2D_{66}\right)m^2n^2\left(\frac{b}{a}\right)^2+D_{22}n^4\right]+\frac{\pi^2}{I^*}\left[N_1\left(\frac{m}{a}\right)^2+N_2\left(\frac{n}{b}\right)^2\right]\left(i=1,2\right) \tag{23}$$

Therefore, the modal coefficients $\alpha_{i,mn}$ are determined by Eq. (14), and Eqs. (21) and (22) can be rewritten in matrix form as Eq. (24),

$$\begin{bmatrix}Q_{11} & Q_{12}\\ Q_{21} & Q_{22}\end{bmatrix}\begin{Bmatrix}\alpha_{1,mn}\\ \alpha_{2,mn}\end{Bmatrix}=\begin{Bmatrix}F\\ 0\end{Bmatrix} \tag{24}$$

$$Q_{11} = \omega_{1,mn}^2 - \omega^2 - \frac{j\omega^2\rho_0}{k_z m^*}\left[\frac{e^{jk_zH}}{e^{-jk_z(h-H)} - e^{-jk_z(H+h)}} - \frac{e^{-jk_zH}}{e^{jk_z(h-H)} - e^{jk_z(H+h)}}\right]$$

$$Q_{12} = \frac{j\omega^2\rho_0}{k_z m^*}\left[\frac{1}{e^{-jk_z(h-H)} - e^{-jk_z(H+h)}} - \frac{1}{e^{jk_z(h-H)} - e^{jk_z(H+h)}}\right]$$

Where:

$$Q_{21} = \frac{j\omega^2\rho_0}{k_z m^*}\left[\frac{e^{jk_zH}}{e^{-jk_z(h-H)} - e^{-jk_z(H+h)}} - \frac{e^{-jk_zH}}{e^{jk_z(h-H)} - e^{jk_z(H+h)}}\right]$$

$$Q_{22} = \omega_{2,mn}^2 - \omega^2 - \frac{j\omega^2\rho_0}{k_z m^*}\left[\frac{1}{e^{jk_z(h-H)} - e^{jk_z(H+h)}} - \frac{1}{e^{-jk_z(h-H)} - e^{-jk_z(H+h)}} + e^{jk_z(H+2h)}\right]$$

$$F = \frac{2j\omega\rho_0 I_{mn}}{m^*}$$

(25)

From which the solution is obtained as Eq. (26).

$$\alpha_{1,mn} = \frac{F.Q_{22}}{Q_{11}.Q_{22} - Q_{12}Q_{21}};\ \alpha_{2,mn} = \frac{-F.Q_{21}}{Q_{11}.Q_{22} - Q_{12}Q_{21}} \qquad (26)$$

III. DEFINITION OF SOUND TRANSMISSION LOSS

The power of incident sound is defined as Eq. (27) [12, 13].

$$\begin{aligned}\Pi_{in} &= \frac{1}{2}\mathrm{Re}\iint_A p_{in}v_{in}^* dA \\ &= \frac{\rho_0\omega^2}{2c_0}\left|4I^2\iint_A e^{-2j\left(k_x x + k_y y\right)}dA - 4I\frac{\omega}{k_z}\sum_{m,n=1}^{\infty}\alpha_{1,mn}\iint_A e^{-j\left(k_x x + k_y y\right)}\phi_{mn}dA + \right. \\ &\qquad \left.\frac{\omega^2}{k_z^2}\sum_{m,n=1}^{\infty}\sum_{k.l=1}^{\infty}\alpha_{1,mn}\alpha_{1,kl}\iint_A \phi_{mn}\left(x,y\right)\phi_{kl}\left(x,y\right)dA\right|\end{aligned} \qquad (27)$$

In a similar manner, the transmitted sound power can be defined as Eq. (28), where p_i^n and p_{tr} are the sound pressures in the incident field and the transmitted field, respectively.

$$\Pi_{tr} = \frac{1}{2}\mathrm{Re}\iint_A p_{tr}v_{tr}^* dA = \frac{\rho_0\omega^4}{2c_0k_z^2}\left|\sum_{m,n=1}^{\infty}\sum_{k,l=1}^{\infty}\alpha_{2,mn}\alpha_{2,kl}\iint_A \phi_{mn}\left(x,y\right)\phi_{kl}\left(x,y\right)dA\right|$$

(28)

The power transmission coefficient can be obtained as Eq. (29).

$$\tau_0\left(\varphi,\theta,f\right) = \frac{\Pi_{tr}}{\Pi_{in}} \qquad (29)$$

The sound transmission loss across the composite sandwich plate is defined by Eq. (30) [12, 13]:

$$STL = 10\log_{10}\left(\frac{1}{\tau_d}\right) \qquad (30)$$

IV. NUMERICAL RESULTS AND DISCUSSION

4.1. Validation

The present analytical approach is validated by comparing with the experimental results of Lu and Xin [7], as shown in Fig. 2 for a finite double-plate excited by wave varying harmonically with incident angle $\varphi = 30°$ and azimuth angle $\theta = 30°$ and thermal load $\Delta T = 0°C$. The double-plate consists of two identical aluminum (isotropic) faceplates with dimensions: a = 0.3 m, b = 0.3 m, h = 0.001 m and air cavity thickness H = 0.08 m. The mechanical properties of aluminum are: E = 70 GPa; ρ = 2700 kg/m³; ν = 0.33. Air properties: c_o = 343 m/s; ρ_o = 1.21 kg/m³; I_o = 1 m²/s.

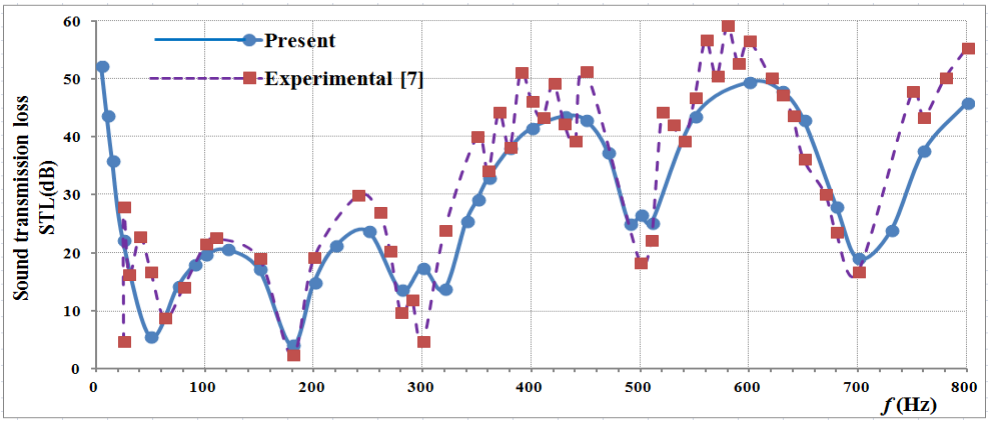

Figure2:Comparison of the present analytical predictions with the experimental results of Lu and Xin [7].

The theoretical predictions of STL in this work agree well with the experimental results of Lu and Xin [7], especially at low frequencies (f < 300 Hz). The obvious difference between theory and experiment occurs in the frequency region f > 300 Hz, due to several factors such as the incident wave may not satisfy the conditions of a plane wave, or the connection of the structure is not perfectly rigid, or due to interference between waves during the experiment.

4.2. Influence of composite materials on STL

The influence of composite materials on STL through a finite simply supported double-composite plate with an air cavity is investigated for an incident sound wave with angle of incidence $\varphi = 30°$, azimuth angle $\theta = 30°$ under thermal load $\Delta T = 20°C$. Four composite materials are selected: Boron/Epoxy, Glass/Epoxy, Graphite/Epoxy and Kevlar/Epoxy. Both faceplates share the laminate configuration $[0/90/0/90]_s$. The geometrical parameters and mechanical properties are given in Table 1.

Table 1: Composite materials properties and geometrical dimensions

Composite	E_1 (GPa)	E_2 (GPa)	G_{12} (GPa)	ν_{12}	ρ (kg/m³)	a×b (m²)	h (m)	H (m)
Boron/Epoxy	204,000	18,500	5,590	0.23	2000	1 × 1	0.005	0.08
Glass/Epoxy	40,851	10,097	3,788	0.27	1946	—	—	—
Graphite/Epoxy	181,000	10,300	7,170	0.28	1600	—	—	—
Kevlar/Epoxy	76,000	5,500	2,300	0.34	1460	—	—	—

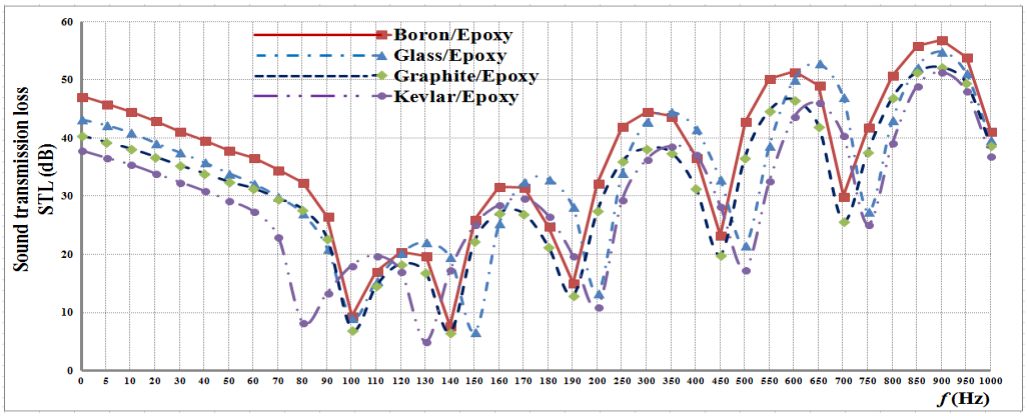

Figure3: Influence of composite materials on STL.

Figure 3 shows that in the low frequency region (f < 100 Hz), the STL value of the double Boron/Epoxy plate is the largest compared to the remaining double-plates and the STL value of the double Kevlar/Epoxy plate is the smallest. In this frequency region, the surface density of the plate is the decisive factor (the control region of stiffness) of the resonance phenomenon of the double-plate structure (plate–air cavity–plate). In the higher frequency region (f > 100 Hz), the peaks and troughs appear more dense and complex,due to the strong interaction between the individual behavior of the single plates (top and bottom) and the overall behavior of the finite double plate system.

4.3. Influence of air cavity thickness (H) on STL

To quantify the influence of air cavity thickness, the STL versus frequency curve is presented in Fig. 4 for a finite double-Glass/Epoxy plate under thermal load $\Delta T = 20°C$. Three values of air cavity thickness are chosen: H = 0.04, 0.06 and 0.08 m. The plate thickness is fixed at h = 0.01 m. Geometrical and material parameters are given in Table 1.

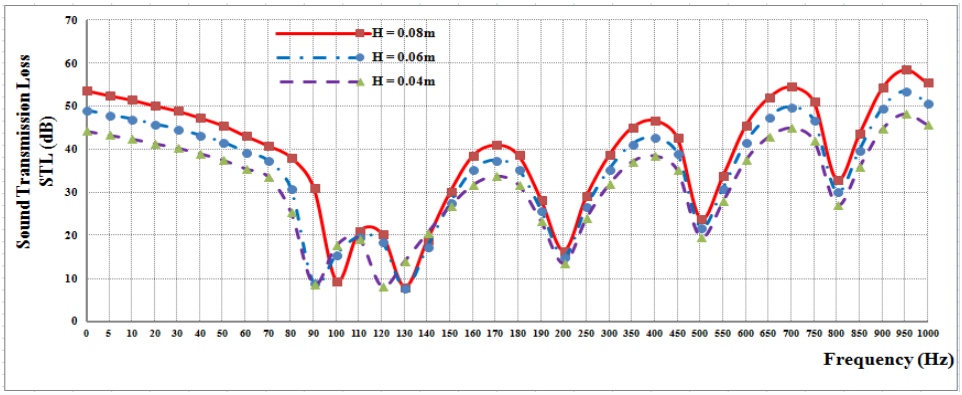

Figure4: Effects of air cavity thickness on STL.

As can be seen in Fig. 4, the position of the first acoustic dip is entirely independent of the air cavity thickness as it is strictly governed by the panel's surface density. Conversely, the second dip shifts prominently toward lower frequencies with increasing cavity thickness, underscoring the dominant role of the plate-cavity-plate resonance. Tailoring this parameter enables effective control and optimization of the acoustic insulation bandwidth for double-panel partitions.

4.4. Influence of lamination scheme on STL

In order to quantify the effects of lamination scheme on STL through the double-composite plate with an enclosed air cavity ($\varphi = 30°$, $\theta = 30°$, $\Delta T = 20°C$), four configurations of the bottom and upper Glass/Epoxy laminated composite plates are selected: $[0/90/0/90]_s$, $[0/0/0/0]_s$, $[90/90/90/90]_s$ and $[90/0/0/90]_s$. Geometrical and material parameters are given in Table 1.

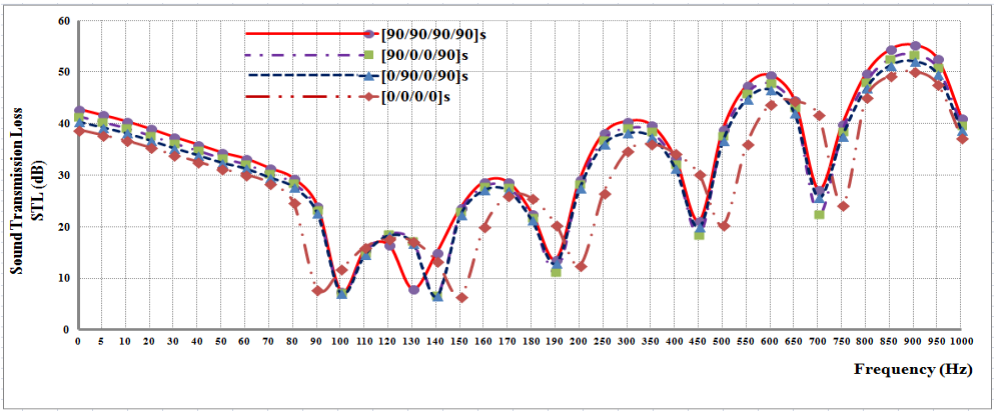

Figure5:Effects of lamination scheme on STL.

From Figure 5, it is clear that the sound transmission loss through the Glass/Epoxy double plate with the $[90/90/90/90]_s$ configuration is greater than that of the plate with the other configurations considered. In the low-frequency region, the first resonance point appears due to the influence of bending stiffness, while the second resonance point appears due to the resonance of the plate–air cavity–plate system. Beyond these frequency regions, the STL curves corresponding to the configurations operate synchronously due to the oscillating behavior of the plate–air cavity–plate system.

V. CONCLUSIONS

In this investigation, an analytical model based on classical laminated plate theory was successfully developed to characterize the sound transmission loss (STL) of a finite, simply supported double-laminated

composite plate enclosing an air cavity under a thermal environment. The primary conclusions drawn from the parametric evaluation are as follows:

- Model Fidelity: The proposed analytical framework is highly reliable, yielding predictions that exhibit excellent agreement with established experimental data, particularly in the low-frequency range ($f < 300$ Hz).
- Material Influence: The surface density of the composite laminates significantly dictates the acoustic insulation in the low-frequency region ($f < 100$ Hz), where the Boron/Epoxy double-panel provides the highest STL and the Kevlar/Epoxy panel yields the lowest.
- Air Cavity Thickness (H) Effect: While the configuration of the first acoustic dip is independent of the air cavity thickness, the second dip shifts prominently toward lower frequencies as the cavity thickness increases due to the dominant role of the plate-cavity-plate resonance.
- Lamination Scheme Effect: The lamination layup heavily influences the vibroacoustic performance. Among the evaluated schemes, the Glass/Epoxy double-panel with a $[90/90/90/90]_s$ configuration exhibits superior sound insulation compared to the $[0/90/0/90]_s$, $[0/0/0/0]_s$, and $[90/0/0/90]_s$ layers.

In summary, the developed analytical approach provides a computationally efficient and accurate alternative to cumbersome numerical models. It serves as a valuable design guideline for tailoring lightweight, high-performance sound-proof double-panel composite configurations operating in thermal environments.

REFERENCES

[1]. W. Kropp and E. Rebillard, "On the air-borne sound insulation of double wall constructions," Acta Acustica United with Acustica, vol. 85, pp. 707–720, 1999.

[2]. M. Villot, C. Guigou, and L. Gagliardini, "Predicting the acoustical radiation of finite size multi-layered structures by applying spatial windowing on infinite structures," Journal of Sound and Vibration, vol. 245, pp. 433–455, 2001.

[3]. R.-J. M. Craik, "Non-resonant sound transmission through double walls using statistical energy analysis," Applied Acoustics, vol. 64, no. 3, pp. 325–341, 2003.

[4]. J.-P. Carneal and C.-R. Fuller, "Active structural acoustic control of noise transmission through double panel systems," AIAA Journal, vol. 33, no. 4, pp. 618–623, 1995.

[5]. P. Carneal and C. R. Fuller, "An analytical and experimental investigation of active structural acoustic control of noise transmission through double panel systems," Journal of Sound and Vibration, vol. 272, pp. 749–771, 2004.

[6]. J.-D. Chazot and J.-L. Guyader, "Prediction of transmission loss of double panels with a patch-mobility method," Journal of Sound and Vibration, vol. 121, pp. 267–278, 2007.

[7]. T. J. Lu and F. X. Xin, Vibro-acoustics of Lightweight Sandwich. Science Press Beijing and Springer-Verlag Berlin Heidelberg, 2014.

[8]. Y. Liu and Y. Li, "Vibration and acoustic response of rectangular sandwich plate under thermal environment," Shock and Vibration, vol. 20, no. 5, pp. 1011–1030, 2013.

[9]. Y. Liu and Y. Li, "Analyses of dynamic response and sound radiation of sandwich plate subjected to acoustic excitation under thermal environment," in 13th International Conference on Fracture, Beijing, China, 2013.

[10]. X. Li et al., "A piecewise shear deformation theory for free vibration of composite and sandwich panels," Composite Structures, vol. 124, pp. 111–119, 2015.

[11]. X. Li and K. Yu, "Vibration and acoustic responses of composite and sandwich panels under thermal environment," Composite Structures, vol. 131, pp. 1040–1049, 2015.

[12]. Pham Ngoc Thanh and Tran Ich Thinh, "Effect of temperature on sound transmission loss of laminated composite plate," Vietnam Journal of Mechanics, vol. 4, pp. 405–417, 2022.

[13]. Tran Ich Thinh and Pham Ngoc Thanh, "Vibroacoustic behavior of a rectangular composite plate in thermal environment," Vietnam Journal of Mechanics, vol. 4, pp. 445–458, 2022.